Hindawi
Adsorption Science & Technology
Volume 2023, Article ID 8217910, 15 pages
https://doi.org/10.1155/2023/8217910

Research Article

$Na_4P_2O_7$-Modified Biochar Derived from Sewage Sludge: Effective Cu(II)-Adsorption Removal from Aqueous Solution

Liangqian Fan,[1,2] **Xianda Wang**,[1,2] **Jiaxin Miao**,[1,2] **Qin Liu**,[1,2] **Jie Cai**,[3] **Xiaochan An**,[1,2] **Fenghui Chen**,[1,2] **Lin Cheng**,[1,2] **Wei Chen**,[1,2] **Hongbing Luo**,[1,2] **Xiaoxiao Zhang**,[1,2] **Ke Zhang**,[1,2] **and Dandan Ma**[1,2]

[1]*College of Civil Engineering, Sichuan Agricultural University, Dujiangyan 611830, China*
[2]*Sichuan Higher Education Engineering Research Center for Disaster Prevention and Mitigation of Village Construction, Sichuan Agricultural University, Dujiangyan 611830, China*
[3]*Department of Physical and Chemical Analysis, Dujiangyan Center for Disease Control and Prevention, Dujiangyan 611830, China*

Correspondence should be addressed to Liangqian Fan; flqjacky@163.com

Received 9 August 2022; Revised 1 October 2022; Accepted 24 November 2022; Published 3 February 2023

Academic Editor: Hesham Hamad

With the rapid development of industrialization, the amount of copper-containing wastewater is increasing, thereby posing a threat to the aquatic ecological environment and human health. Sludge biochar has received extensive concern in recent years due to its advantages of low cost and sustainability for the treatment of heavy-metal-containing wastewater. However, the heavy-metal-adsorption capacity of sludge biochar is limited. This study prepared a sodium pyrophosphate- ($Na_4P_2O_7$-) modified municipal sludge-based biochar (SP-SBC) and evaluated its adsorption performance for Cu(II). Results showed that SP-SBC had higher yield, ash content, pH, Na and P content, and surface roughness than original sewage sludge biochar (SBC). The Cu(II)-adsorption capacity of SP-SBC was 4.55 times than that of SBC at room temperature. For Cu(II) adsorption by SP-SBC, the kinetics and isotherms conformed to the pseudo-second-order model and the Langmuir–Freundlich model, respectively. The maximum adsorption capacity of SP-SBC was 38.49 $mg \cdot g^{-1}$ at 35°C. Cu(II) adsorption by SP-SBC primarily involved ion exchange, electrostatic attraction, and precipitation. The desired adsorption performance for Cu(II) in the fixed-bed column experiment indicated that SP-SBC can be reused and had good application potential to treat copper-containing wastewater. Overall, this study provided a desirable sorbent (SP-SBC) for Cu(II) removal, as well as a new simple chemical-modification method for SBC to enhance Cu(II)-adsorption capacity.

1. Introduction

With the rapid development of industrialization, the heavy metals that enter the water environment through human activities inevitably increase [1–3]. Due to the persistence, bioaccumulation, pathogenicity, and carcinogenicity of heavy metals, the water-environment pollution they cause is attracting extensive attention [1, 4]. Copper, as an important heavy metal material, is widely used in the fields of electronics, energy, communications, and machinery production, resulting in a large amount of copper-containing wastewater. The concentration of copper in the wastewater varies from tens to thousands of milligrams per liter [5]. Once the wastewater is directly discharged into natural water bodies without proper treatment, it harms aquatic organisms and leads to a series of health problems to humans, such as nausea, diarrhea, liver, and kidney damage [1, 6]. Thus, the removal of copper from wastewater has become an important issue for heavy-metal pollution control. Several methods are presently used to deal with copper-containing wastewater, primarily including chemical precipitation, bioremediation, membrane separation, and adsorption [7]. Among these methods, adsorption has elicited extensive attention in view of its advantages of convenient operation, considerable efficiency, low cost, and strong anticontamination ability [8, 9]. For adsorption, sorbent development is an important research task [10–14].

Biochar is a porous and carbon-rich solid material obtained by pyrolyzing biomass under anoxic or anaerobic conditions [15, 16]. Due to the high porosity, large surface area, rich surface functional groups, and high pH value of biochar, it receives extensive attention in the field of heavy-metal-containing wastewater treatment [17]. In previous years, a large number of biochar materials such as discarded mushroom-stick biochar [18], corn straw biochar [19], date seed biochar [20], tobacco stem biochar [21], industrial alkali lignin biochar [22], and *Ascophyllum nodosum* seaweed biochar [23] have been successfully prepared to remove heavy metal from wastewater. These studies show that biochar is an environmentally friendly and cost-effective adsorption material for heavy-metal adsorption. With the deepening of research, some scholars have performed studies on biochar modification, particularly chemical modification, to improve the heavy-metal-adsorption capacity by raw biochar [24–31]. These studies have indicated that the heavy-metal-adsorption capacity of biochar can be significantly improved by an effective modifier. Such a modifier adds adsorption sites and enhances electrostatic attraction, surface complexation, or surface precipitation on biochar.

In China, the growing sewage sludge produced from sewage treatment has become a serious burden on ecology and society [32]. Accordingly, China has the urgent need for environment-friendly methods to realize the effective treatment of sewage sludge. However, the commonly used methods of incineration, sanitary landfilling, and land application [32] have some shortcomings that could lead to secondary pollution. For example, NO_x, SO_2, and volatile heavy metals produced from incineration can cause serious air pollution [33]. Sanitary landfilling can occupy land. Direct agricultural application may harm living organisms [34]. Many researchers have reported the related studies on converting sewage sludge to biochar for the treatment of heavy-metal-containing wastewater [35–41]. They found that preparing biochar from sewage sludge can realize the harmless and reductive treatments of sewage sludge and obtain a low-cost and sustainable sorbent for the treatment of heavy-metal-containing wastewater. However, the heavy-metal-adsorption capacity of sludge-based biochar is unsatisfactory, which limits its promotion and application to a certain extent [42, 43]. Some modifiers such as Fe_3O_4 [44], nanostructured $CaCO_3$ [45], trithiocyanuric acid trisodium salt [46], α-Fe_2O_3 and α-FeOOH [47], K_2FeO_4 [48], and hydroxyapatite [42] have been successfully applied to prepare modified sewage sludge biochar, and satisfactory heavy-metal-adsorption capacity has been achieved. At present, chemical modification is a noteworthy research direction for improving the adsorption capacity of heavy metals by sewage sludge biochar [45, 49]. In the present study, we used sodium pyrophosphate ($Na_4P_2O_7$), an additive widely used in the food industry, water industry, and daily chemical industry, as a modifier to prepare $Na_4P_2O_7$-modified sewage sludge-based biochar (SP-SBC). The desirable Cu(II)-adsorption capacity of SP-SBC was hoped to be achieved through the precipitation between pyrophosphate or phosphate and Cu(II). Although some similar reports exist on sewage sludge biochar modified with chemical modification for Cu(II) adsorption [42, 50, 51], to our knowledge, SP-SBC and its Cu(II)-adsorption performance are reported herein for the first time. Moreover, our one-pot preparation method of SP-SBC was simpler than those of biochars reported by Chen et al. [42], Phoungthong and Suwunwong [50], and Tang et al. [51]. This study could provide an alternative path for modifying sewage sludge biochar, which is beneficial to promote the practical application of sludge biochar.

The aims of this study were as follows: (i) to prepare SP-SBC and explore its properties, (ii) to investigate the adsorption behaviors of SP-SBC for Cu(II), and (iii) to understand the application potential of SP-SBC for Cu(II)-adsorption removal. Herein, SP-SBC was prepared. The properties of SP-SBC and original sewage sludge biochar (SBC) were characterized by the yield; ash content; pH, K, Ca, Na, Mg, and P contents; SEM; and FTIR. Then, the effects of sorbent dosage, initial pH, ionic strength, contact time, and temperature on the Cu(II) adsorption by SP-SBC were determined by batch-adsorption experiments. For Cu(II) adsorption by SP-SBC, the kinetics and isotherms were explored. Lastly, a fixed-bed column experiment was performed.

2. Materials and Methods

2.1. Materials. Sodium pyrophosphate ($Na_4P_2O_7$; AR, 99%), copper nitrate trihydrate ($Cu(NO_3)_2{\cdot}3H_2O$; AR, 99%), sodium nitrate ($NaNO_3$; AR, 99%), silica sand, nitric acid (HNO_3; AR, 65–68 wt%), and sodium hydroxide (NaOH, AR, 98%) were all supplied by Kelong Chemical Co., Ltd. (Chengdu, China) without further purification. Ultrapure water (18.25 MΩ) was used to prepare the used solutions. Sewage sludge was acquired from a local municipal wastewater-treatment plant in Chengdu city, China.

2.2. Preparation of Biochar. SP-SBC was prepared with a one-pot method (Figure 1). The specific procedures were as follows. Sewage sludge was ground and sieved to pass a 10-mesh sieve after natural drying. A part of sieved sludge was impregnated with $Na_4P_2O_7$ (60 g·L^{-1}) at a ratio of 1/20 (mass/volume) for 12 h in a constant-temperature shaker under the conditions of 25°C and 130 rpm. Afterwards, the impregnated sludge was dried at 60°C until the weight was stable. The dried impregnated sludge and the other part of the sieved sludge were loaded into different ceramic crucibles, sealed, and capped. Then, they were pyrolyzed for 2 h at 400°C in a muffle furnace. After grinding the pyrolyzed product of the original sludge and sieving (60 mesh), the acquired particles under the sieve were recorded as SBC. The pyrolyzed product of the impregnated sludge was washed several times with 55–65°C deionized water and dried at 60°C until the weight was stable. The dried product was passed through a sieve (60 mesh) after grinding. The obtained particles under the sieve were recorded as SP-SBC.

2.3. Properties of Biochar. The analysis methods for the properties of SBC or SP-SBC were as follows. Equation (1)

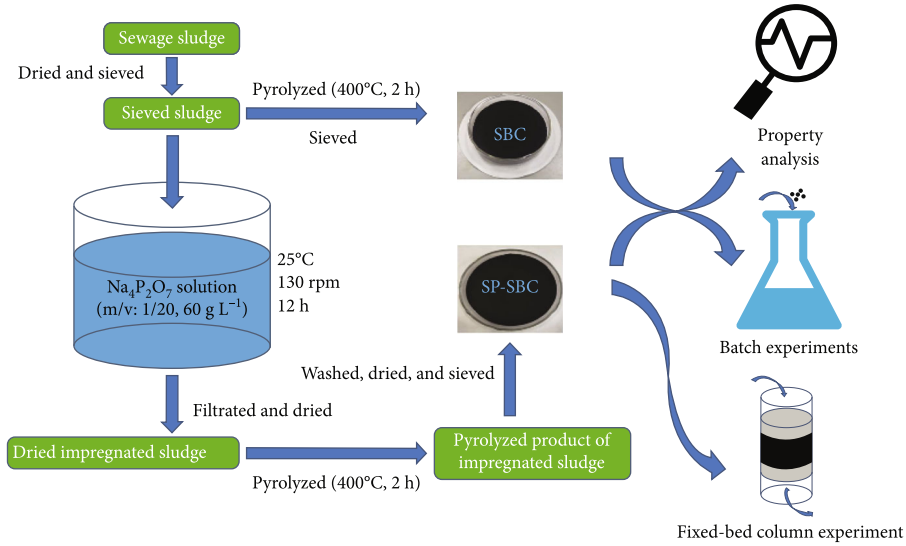

Figure 1: Flow chart of SP-SBC preparation.

Table 1: Specific conditions for each batch experiment.

Batch experiment	Experimental conditions					
	Sorbent dosage (g)	Initial solution pH	Ionic strength ($NaNO_3$, M)	Contact time (h)	Temperature (°C)	Cu(II) concentration ($mg \cdot L^{-1}$)
Sorbent dosage	0.025, 0.05, 0.075, 0.1, 0.2, 0.3, 0.5	5	0	12	25	50
Initial solution pH	0.1	3, 3.5, 4, 4.5, 5, 6	0	12	25	50
Ionic strength	0.1	5	0, 0.005, 0.01, 0.03, 0.05, 0.08, 0.10, 0.50	12	25	50
Contact time	0.1	5	0	0.5, 1, 2, 3, 4, 6, 8, 10, 12, 14	25	50
Temperature	0.1	5	0	12	15, 25, 35	50, 150, 200, 300, 400, 600

was used to calculate the yield (Y, %):

$$Y = \left(\frac{m_0}{m_t}\right) \times 100\%, \quad (1)$$

where m_0 and m_t denote the weight of SBC (or SP-SBC) and sewage sludge (g), respectively. Ash content was detected by burning 1.00 g of samples in a muffle furnace at 700°C for 2 h and calculated by the following equation:

$$\text{Ash}(\%) = \left(\frac{M_0}{M_t}\right) \times 100\%, \quad (2)$$

where M_0 and M_t represent the weight of SBC (or SP-SBC) after and before burning (g), respectively. The pH; contents of Na, K, Ca, Mg, and P; and the surface structural morphology (i.e., SEM images) were determined as in our previous methods [52]. The surface functional groups on SBC, SP-SBC, and SP-SBC after Cu(II) adsorption (SP-SBC+Cu) were recorded with a Nicolet iS50-type FTIR spectroscope (Thermo Fisher Scientific, Inc., Waltham, USA). At different solution pH values, the zeta potentials of SP-SBC were measured based on our previous methods to calculate the isoelectric point (pH_{IEP}) [52].

2.4. Batch Experiments. The influences of sorbent dosage, initial solution pH, ionic strength, contact time, and temperature on Cu(II) adsorption by SP-SBC were determined with batch experiments. For all batch experiments, the Cu(II) solution with a preset concentration was prepared by diluting 1000 $mg \cdot L^{-1}$ of Cu(II) stock solution, which was in turn prepared with $Cu(NO_3)_2 \cdot 3H_2O$ and ultrapure water (18.25 MΩ). In a typical procedure, a certain amount of SP-SBC was mixed with 50 mL of Cu(II) solution with a designed concentration, followed by adjusting the pH to a predesigned value. Then, the mixture was shaken for a certain time period at a preset temperature and at 130 rpm in a constant-temperature shaker. The specific conditions for each batch experiment are shown in Table 1. Furthermore,

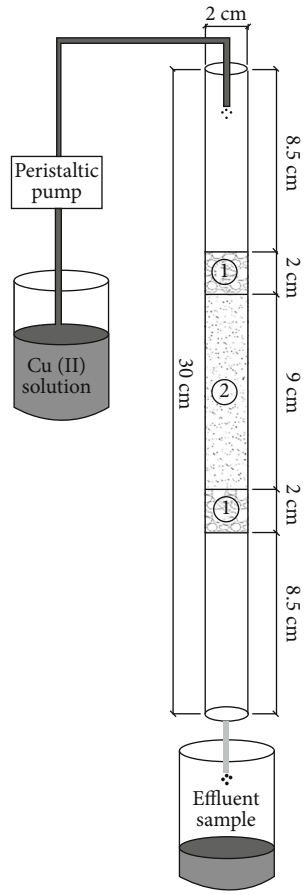

Figure 2: Sketch of fixed-bed column device (①: 2 cm thick quartz sand-packed layer; ②: 9 cm thick SP-SBC-packed layer).

Table 2: Some properties of SBC and SP-SBC.

Items	SBC	SP-SBC
Yield (%)	60.57 ± 0.17	68.34 ± 0.21
Ash content (%)	66.77 ± 0.39	75.23 ± 0.33
pH value	8.13 ± 0.03	10.54 ± 0.05
Na ($mg{\cdot}g^{-1}$)	1.76 ± 0.41	31.72 ± 1.97
K ($mg{\cdot}g^{-1}$)	6.81 ± 0.36	3.68 ± 0.28
Ca ($mg{\cdot}g^{-1}$)	27.48 ± 0.57	20.63 ± 2.57
Mg ($mg{\cdot}g^{-1}$)	7.87 ± 0.18	5.34 ± 0.38
P ($mg{\cdot}g^{-1}$)	24.94 ± 1.46	40.86 ± 3.32

SP-SBC was replaced by SBC and subjected to the same experiment processes in the batch experiment of the effect of contact time to compare the difference in adsorption capacity between SP-SBC and SBC.

Once a batch experiment was completed, the mixture was taken out and the suspension was passed through a 0.45 μm microfiltration membrane. In the filtrate, the Cu(II) concentration was tested with a PinAAcle900T-type flame atomic adsorption spectrophotometer (FAAS) (PerkinElmer Instrument Co., Ltd., Akron, USA). Then, Equation (3) was used to calculate the Cu(II)-adsorption capacity (q_e):

$$q_e = \frac{0.05(C_0 - C_e)}{W}, \tag{3}$$

where C_0 refers to the initial Cu(II) concentration ($mg{\cdot}L^{-1}$) at the beginning of experiment, C_e refers to the detected Cu(II) concentration ($mg{\cdot}L^{-1}$) at the end of experiment, and W is the amount of biochar (g).

2.5. Adsorption Kinetics and Isotherms. For Cu(II) adsorption by SP-SBC, the acquired data in the batch experiment of the effect of contact time were simulated with the pseudo-first-order (PFO) model, the pseudo-second-order (PSO) model, and the intraparticle diffusion (IPD) model (Equations (4)–(6)) to analyze the kinetic characteristics [12].

$$Q_t = Q_{\text{et}}\left(1 - e^{-k_1 t}\right), \tag{4}$$

$$Q_t = \frac{t{Q_{\text{et}}}^2 k_2}{1 + tQ_{\text{et}}k_2}, \tag{5}$$

$$Q_t = k_i t^{1/2} + C, \tag{6}$$

where Q_{et} is the adsorption capacity ($mg{\cdot}g^{-1}$) at equilibrium and Q_t is the adsorption capacity ($mg{\cdot}g^{-1}$) at time t. k_1, k_2, and k_i denote the constants of the PFO model (h^{-1}), the PSO model ($g{\cdot}mg^{-1}{\cdot}h^{-1}$), and the rate constant of the IPD diffusion ($mg{\cdot}(g{\cdot}min^{0.5})^{-1}$), respectively. C indicates the boundary-layer thickness ($mg{\cdot}g^{-1}$). The acquired data in the batch experiment of the effect of temperature was matched with the Langmuir (L) model, the Freundlich (F) model, the Langmuir–Freundlich (L-F) model, and the Dubinin–Radushkevich (D-R) model (Equations (7)–(12)) [16, 53–56] to explain the adsorption isotherms, respectively.

$$Q_e = \frac{Q_m K_L C_e}{1 + K_L C_e}, \tag{7}$$

$$Q_e = K_f {C_e}^{1/n}, \tag{8}$$

$$Q_e = \frac{Q_m (K_a C_e)^{n'}}{1 + (K_a C_e)^{n'}}, \tag{9}$$

$$\varepsilon = \text{RTln}\left(1 + \frac{1}{C_{\text{eD}}}\right), \tag{10}$$

$$Q_{\text{eD}} = Q_{\text{mD}} \exp\left(-\beta\varepsilon^2\right), \tag{11}$$

$$E = \frac{1}{\sqrt{2\beta}}, \tag{12}$$

where K_L is the constant of the L model ($L{\cdot}mg^{-1}$). K_f is the constant of the F model ($mg^{(1-n)}{\cdot}L^n{\cdot}g^{-1}$). $1/n$ is an empirical constant representing adsorption intensity. K_a is the constant of the L-F model ($L{\cdot}mg^{-1}$), which can be used to reflect

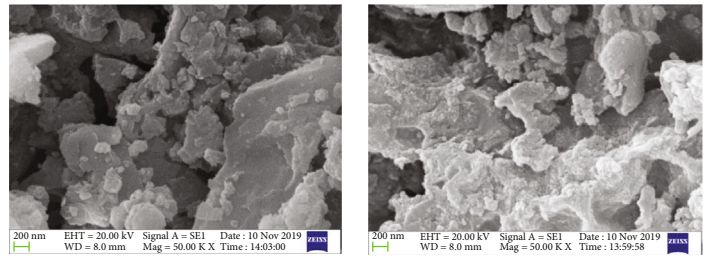

Figure 3: SEM image of biochar: (a) SBC and (b) SP-SBC.

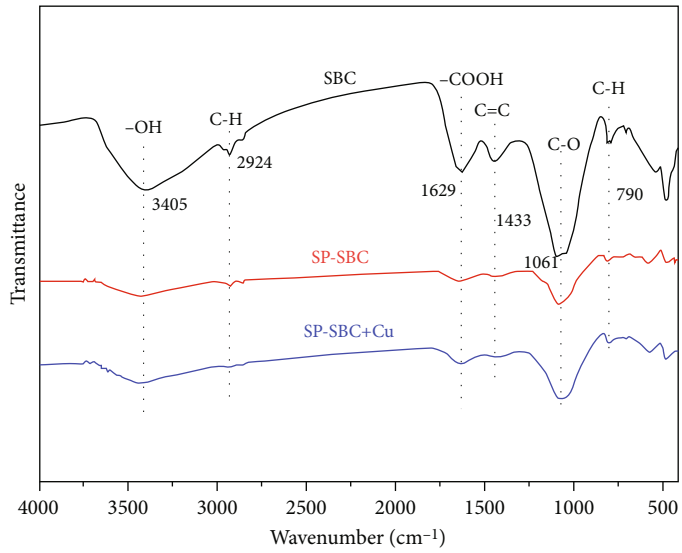

Figure 4: FTIR spectra of SBC, SP-SBC, and SP-SBC+Cu.

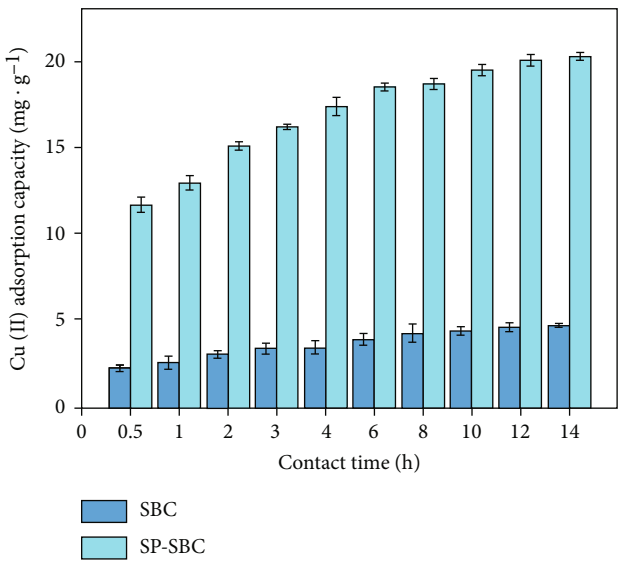

Figure 5: Adsorption capacities of SBC and SP-SBC for Cu(II) at different contact times.

the adsorption affinity. n' is the heterogeneity factor. Q_e is the equilibrium adsorption capacity at the end of the experiment (mg·g^{-1}). Q_m is the maximum adsorption capacity (mg·g^{-1}). ε is the Polanyi potential constant (J·mol^{-1}). C_{ed} is the detected Cu(II) concentrations (mol·L^{-1}) at the equilibrium. Q_{eD} and Q_{mD} are the equilibrium adsorption capacity (mol·g^{-1}) and the maximum adsorption capacity (mol·g^{-1}), respectively. R is the gas constant (8.314 J·(mol·K)$^{-1}$). T is the absolute temperature (K).

2.6. Fixed-Bed Column Experiment. A fixed-bed column experiment was conducted to understand the application potential of SP-SBC for Cu(II) adsorption. The sketch map of the fixed-bed column device is shown in Figure 2. Four cycles were performed in the fixed-bed column experiment. Each cycle included two processes, i.e., adsorption process and desorption process. For the adsorption process, the Cu(II) solution (C_{in} = 50 mg · L^{-1}, pH 5) was pumped into the top of the column (flow rate (Q) = 15 mL · min^{-1}). The effluent samples were collected every 15 min, and the Cu(II) concentrations of samples (C_{en}, mg·L^{-1}) were measured by the FAAS to draw the breakthrough curve. Based on the acquired breakthrough curve, the total inputted Cu(II) amount (M, mg), total Cu(II)-adsorption amount (M', mg), volume of treated Cu(II) solution (V_{eff}, mL), and equilibrium adsorption capacity of SP-SBC (q_{ec}, mg·g^{-1}) were calculated by Equations (13)–(16), respectively. For the desorption process, a certain volume of 0.5 M NaOH

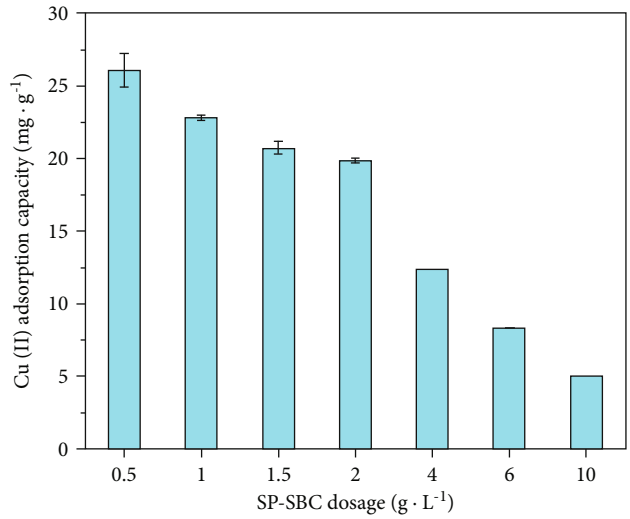

Figure 6: Effect of SP-SBC dosage on the adsorption capacity of SP-SBC for Cu(II).

solution was added to the fixed-bed column until the solution level was kept above the top quartz sand-packed layer. After soaking for 12 h, the fixed-bed column was rinsed with ultrapure water several times until the eluent pH was about neutral. Then, the regenerated fixed-bed column reactor was obtained. The regenerated fixed-bed column was reused for the next cycle.

$$M = \frac{Qt_eC_{\text{in}}}{1000}, \tag{13}$$

$$M' = \frac{Q}{1000}\int_0^{t_e}(C_{\text{in}} - C_{\text{en}})\text{dt}, \tag{14}$$

$$V_{\text{eff}} = Qt_e, \tag{15}$$

$$q_{\text{ec}} = \frac{M'}{m}, \tag{16}$$

where t_e is the adsorption saturation time (min), which is the corresponding time when $C_t/C_0 = 0.9$ [57, 58]. m is the SP-SBC mass packed in the experimental device (g).

2.7. Statistical Analysis. To ensure the reliability of experimental data, all experiments were repeated three times in this study. Origin 8.0 was used for plotting. SPSS Statistics 23.0 was used to analyze the experimental data.

3. Results and Discussion

3.1. Properties of SBC and SP-SBC. The property parameters of SBC and SP-SBC are shown in Table 2. The yields of SBC and SP-SBC were 60.57% and 68.34%, respectively, which were close to those of other sludge biochars prepared at the same pyrolysis temperature [59, 60]. Compared with those of SBC, the Na and P contents of SP-SBC significantly increased ($p < 0.05$), indicating that pyrophosphate was successfully introduced onto SP-SBC. However, the K, Ca, and Mg contents of SP-SBC decreased, which may be related to the dilution effect resulting from the increase in Na and P contents after modification. The ash content of SP-SBC was higher ($p < 0.05$) than that of SBC, which was due to the introduction of Na and P elements after modification. The alkalinity of SP-SBC was higher than that of SBC, which could be attributed to the increase in ash content and the alkalinity of the sodium pyrophosphate solution.

Figure 3 shows the scanning electron microscopy (SEM) images of SBC and SP-SBC, which reflected the surface structural morphology. The SP-SBC surface (Figure 3(b)) was rougher than that of SBC (Figure 3(a)) and filled with many microparticles, which was caused by the introduction of sodium pyrophosphate. The results of FTIR spectra of SBC and SP-SBC (Figure 4) revealed peaks at around 790 and 1061 cm^{-1}, which were due to the aromatic C-H out-of-plane vibrations [61] and C-O stretching vibration, respectively [15, 62, 63]. The peak at around 1433 cm^{-1} represented the C=C stretching vibration of aromatic hydrocarbons [64]. The peak at 1629 cm^{-1} was associated with the –COOH stretching vibration [65]. The observed peak at around 2924 cm^{-1} represented the C-H stretching vibration [66]. The intense peak at around 3405 cm^{-1} was due to the -OH stretching vibration [67]. Overall, the peaks of the two biochars were consistent, suggesting that the categories of functional groups did not change before and after modification. However, for SP-SBC, the intensities of these peaks weakened. These results suggested that the amounts of the functional groups on the SP-BC surface (especially for –OH and –COOH) decreased. This finding was consistent with the above result that the alkalinity of SP-SBC was higher than that of SBC.

3.2. Adsorption Capacities of SBC and SP-SBC for Cu(II). The adsorption capacities of SBC and SP-SBC for Cu(II) varied with increased contact time (Figure 5). For SBC, the Cu(II)-adsorption capacity tended to be stable after 10 h. For SP-SBC, the Cu(II)-adsorption capacity tended to reach equilibrium at 12 h. At adsorption equilibrium, SP-SBC and SBC achieved the Cu(II)-adsorption capacities of 20.01 and 4.40 $\text{mg}\cdot\text{g}^{-1}$, respectively. Results showed that SP-SBC had a higher Cu(II)-adsorption capacity (4.55 times) than SBC. First, the surface of SP-SBC was rougher than that of SBC (Figure 3), which helped in increasing the contact of Cu(II) with SP-SBC [68]. Second, for SP-SBC, the increased equivalent of sodium was greater than the sum of the decreased equivalents of potassium, calcium, and magnesium (Table 2), which enhanced the ion exchange with Cu(II) [52]. Third, the significant increase in the phosphorus and alkalinity of SP-SBC (Table 2) led to increased copper precipitation [69]. The above three reasons caused the significant improvement in the Cu(II)-adsorption capacity of SP-SBC.

For Cu(II) adsorption by biochar, the complexation and π electron coordination of surface functional groups may be involved [6, 70, 71]. In the Section 3.1, compared with SBC, SP-SBC had fewer surface functional groups. However, the Cu(II)-adsorption capacity of SP-SBC was 4.55 times higher than that of SBC. This finding indicated that the increased Cu(II)-adsorption capacity of SP-SBC was independent of

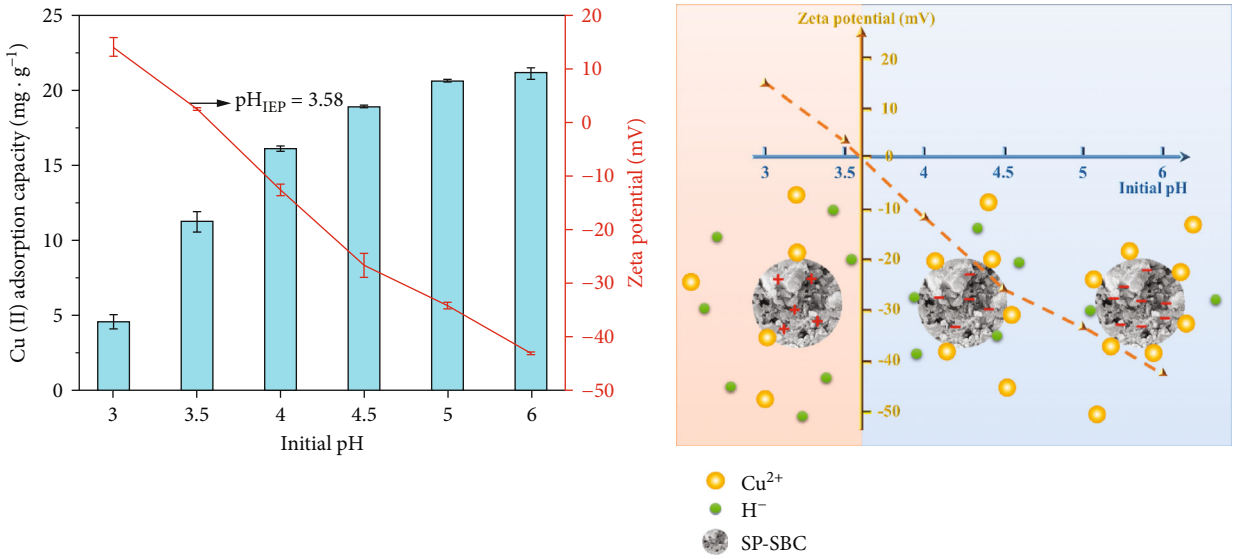

Figure 7: (a) Effect of initial pH on the adsorption capacity of SP-SBC for Cu(II), and (b) an illustration of the effect of initial pH on Cu(II) adsorption by SP-SBC.

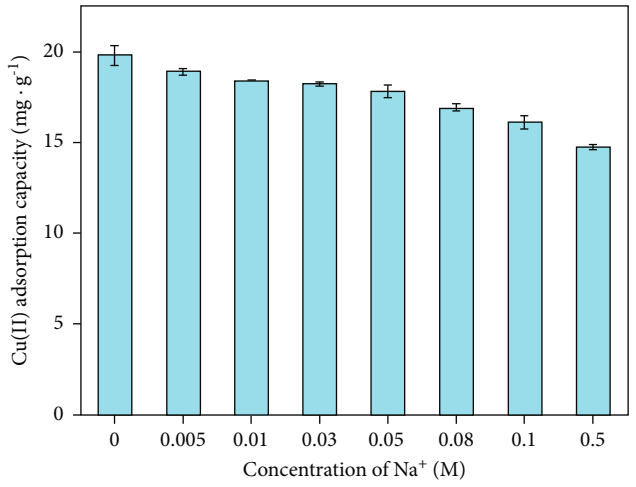

Figure 8: Effect of ionic strength on the adsorption capacity of SP-SBC for Cu(II).

surface functional groups. Thus, the complexion and π electron coordination of surface functional groups may not be the main mechanism for the Cu(II) adsorption by SP-SBC. Additionally, the SP-SBC after Cu(II) adsorption (SP-SBC +Cu) was characterized by FTIR (Figure 4). We found inconspicuous changes in the positions and intensities of peaks between the FTIR spectra of SP-SBC and SP-SBC +Cu. These results suggested that surface functional groups had little effect on Cu(II) adsorption, which strongly supported the above discussion of surface functional group effects for Cu(II) adsorption.

Overall, modifying SBC with sodium pyrophosphate can effectively improve its Cu(II)-adsorption capacity.

3.3. Effect of SP-SBC Dosage. For the Cu(II)-adsorption capacity, the influence of SP-SBC dosage is shown in Figure 6. With increased SP-SBC dosage (from 0.5 g·L^{-1} to 10 g·L^{-1}), the Cu(II)-adsorption capacity decreased ($p < 0.05$) from 26.06 mg·g^{-1} to 4.983 mg·g^{-1}, in accordance with those of other reported biochars [71, 72]. This decrease in adsorption capacity for Cu(II) was associated with the following reasons: (i) the nonsaturated Cu(II) adsorption on SP-SBC caused by the excessive amount of SP-SBC [72] and (ii) the agglomeration and polymerization of SP-SBC at a high dosage [73].

3.4. Effect of Initial pH. To avoid the experimental interference caused by the extra precipitation of Cu(II) at the initial pH of >6 [6, 69], the initial pH was adjusted to 3–6. Figure 7(a) shows the effect of initial pH on the Cu(II) adsorption by SP-SBC. As shown in Figure 7, with increased initial pH from 3 to 5, the Cu(II)-adsorption capacity rapidly increased from 4.52 mg·g^{-1} to 20.63 mg·g^{-1} ($p < 0.05$). pH importantly influences the adsorption of metal ions because it usually determines the surface charge of the sorbent [3, 6, 12, 23]. Figure 7 also displays the zeta potentials of SP-SBC at different pH values. We found that the zeta potential gradually decreased with increased initial pH ($p < 0.05$), and the isoelectric point (pH$_{IEP}$) of SP-SBC was 3.58. These results suggested that the negative charges on the surface of SP-SBC increased with increased pH to >3.58. It enhanced the electrostatic attraction between Cu(II) and SP-SBC, leading to the increasing trend of Cu(II)-adsorption capacity from the initial pH of 3 to 5 [4, 15]. Moreover, the adsorption competition between Cu(II) and H^{+} gradually weakened with increased initial pH within the range of 3–5, also resulting in increased Cu(II)-adsorption capacity of SP-SBC. These findings suggested that electrostatic attraction participated in the adsorption of Cu(II) by SP-SBC (Figure 7(b)). When the initial pH was above 5, the Cu(II)-

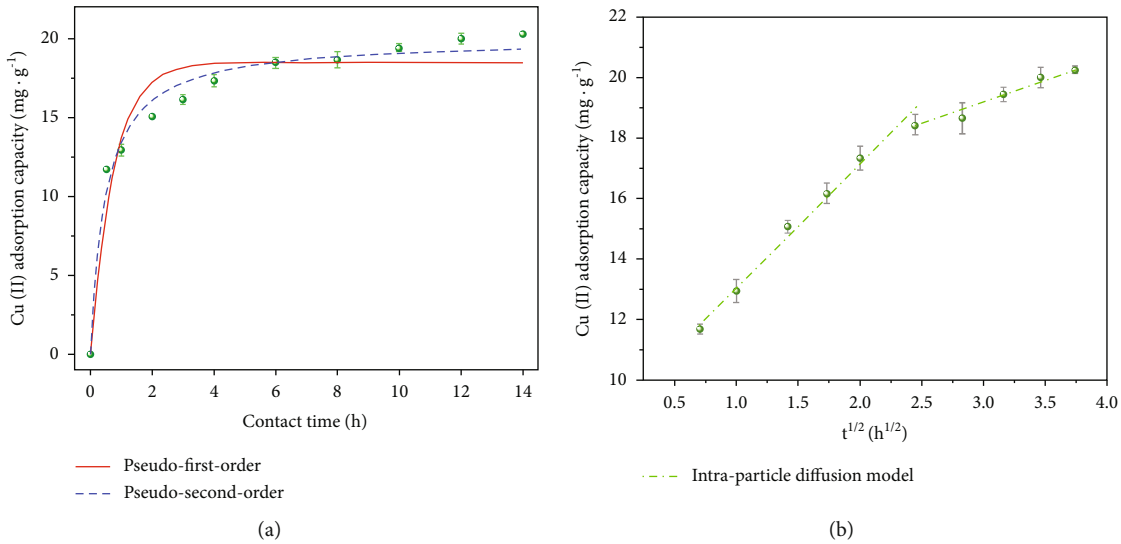

Figure 9: Effect of contact time on the adsorption capacity of SP-SBC for Cu(II) and fitting results of the PFO and PSO models (a) and the IPD model (b).

Table 3: Fitting parameters of three kinetic models.

Pseudo-first order			Pseudo-second order		
Q_{et} (mg·g^{-1})	k_1 (h^{-1})	R^2	Q_{et} (mg·g^{-1})	k_2 (g·mg^{-1}·h^{-1})	R^2
18.50	1.348	0.931	20.02	0.103	0.980
Intraparticle diffusion					
Step 1			Step 2		
C (mg·g^{-1})	k_i (mg·(g·min$^{0.5}$)$^{-1}$)	R^2	C (mg·g^{-1})	k_i (mg·(g·min$^{0.5}$)$^{-1}$)	R^2
8.91	4.12	0.98	14.91	1.43	0.95

adsorption capacity remained unchanged ($p > 0.05$), consistent with the results of Deng et al. [74].

3.5. Effect of Ionic Strength. Ionic strength usually has a significant effect on adsorption [75]. The effect of ionic strength (Na^+) on Cu(II) adsorption by SP-SBC is displayed in Figure 8. With increased ionic strength (0.005–0.5 M), the Cu(II)-adsorption capacity decreased significantly ($p < 0.05$). The reasons for this trend were as follows: (i) Na^+ competed with Cu^{2+} in the adsorption [6]; (ii) a dense hydrating shell formed on the surface of SP-SBC once Na^+ was adsorbed [76], which prevented Cu(II) from making contact with the surface of SP-SBC; and (iii) the increase in ionic strength greatly reduced the activity coefficient of Cu(II), making it difficult for SP-SBC to capture Cu(II) [77]. In conclusion, ionic strength can significantly influence the Cu(II)-adsorption capacity of SP-SBC, especially under the high-ionic-strength condition. These results suggested that attention should be paid to the salinity control for the application of SP-SBC in high-salinity copper-containing wastewater.

3.6. Effect of Contact Time and Adsorption Kinetics. Figure 9 shows the effect of contact time on Cu(II) adsorption by SP-SBC. With increased contact time, the Cu(II)-adsorption capacity increased ($p < 0.05$) within the initial 12 h and then reached equilibrium ($p > 0.05$) (Figure 9). The Cu(II) adsorption by SP-SBC was fast within the initial 0.5 h, and the adsorption capacity at 0.5 h reached 58% of the adsorption capacity at equilibrium time. Then, the Cu(II)-adsorption rate gradually slowed down between 0.5 and 12 h, finally reaching stability after 12 h. The high initial Cu(II)-adsorption rate was due to the considerable amount of unsaturated adsorption sites on SP-SBC, whereas the decelerating adsorption rate was due to the adsorption sites being gradually saturated as adsorption proceeded [23].

Figure 9 exhibits the fitting curves of the PFO, PSO, and IPD models for Cu(II) adsorption by SP-SBC. The fitting curve of the PSO model showed a better approximation to the experimental data than those of the PFO and IPD models. The fitting parameters, i.e., Q_{et}, k_1, k_2, k_i, C, and correlation coefficient (R^2), are displayed in Table 3. Compared with the PFO and IPD models, the PSO model had the highest R^2 (0.980). Additionally, the simulated Q_{et} (20.02 mg·g^{-1}) obtained by the PSO model better agreed with the q_e (20.01 mg·g^{-1}) obtained in the experiment. Therefore, Cu(II) adsorption by SP-SBC was better depicted by the PSO model. The result implied that the number of active sites of the SP-SBC surface restricted the Cu(II)-adsorption rate of SP-SBC; i.e., chemical adsorption was the rate-limiting step for Cu(II) adsorption by SP-SBC [15, 78, 79]. Thus,

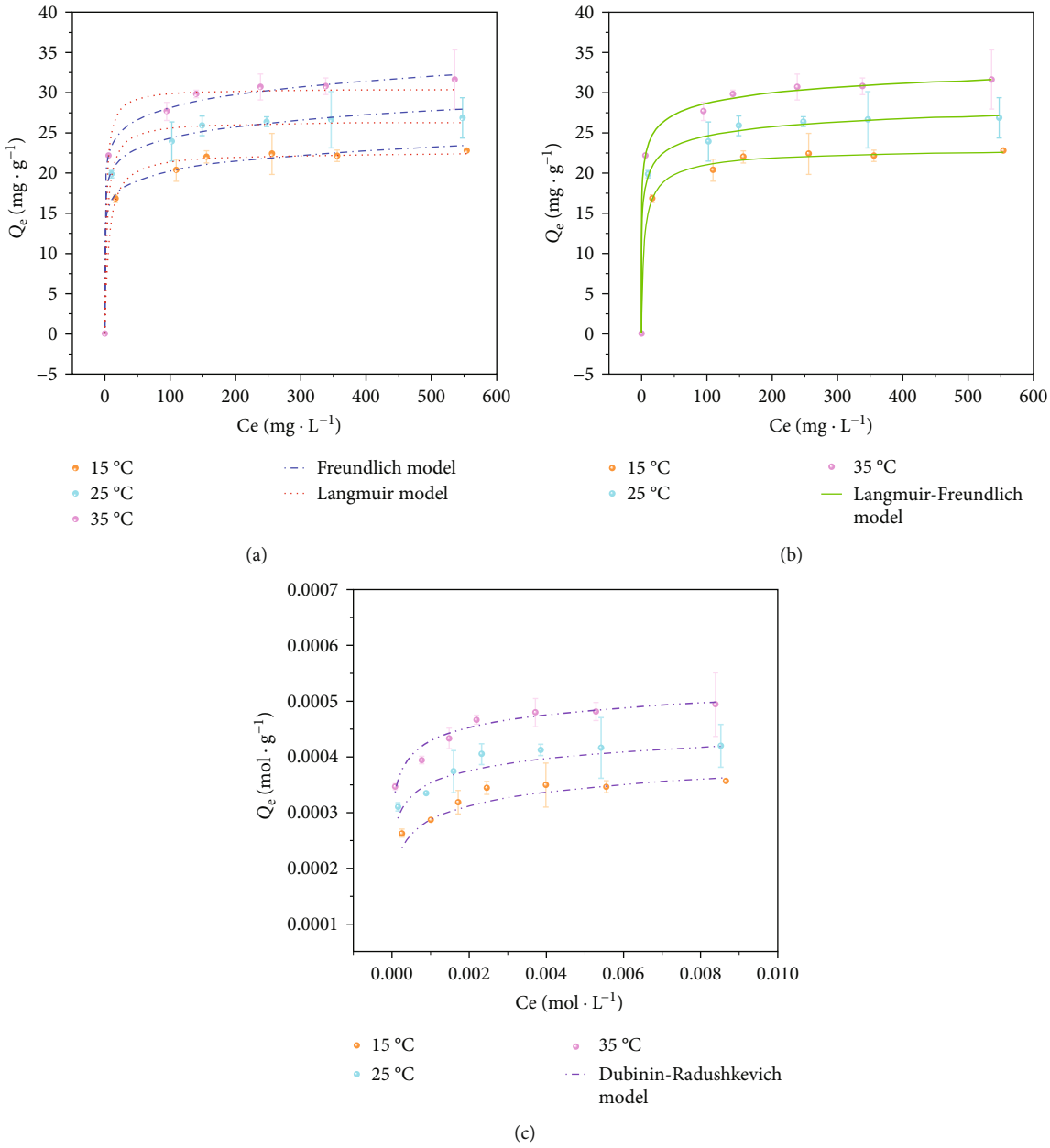

Figure 10: Effect of temperature on the adsorption capacity of SP-SBC for Cu(II), and fitting results of the F and L (a), L-F (b), and D-R (c) models.

chemical adsorption may be a key mechanism in this study [11, 13, 71], consistent with the discussion in Section 3.2. Meanwhile, Figure 9(b) shows that the adsorption process of Cu(II) by SP-SBC can be divided two stages: boundary-layer diffusion with fast diffusion speed and intraparticle diffusion with relatively slow diffusion speed. Notably, the fitting curves of the above two stages did not pass through the original point, indicating that intraparticle diffusion was not the only rate-limiting step to control the Cu(II)-adsorption process of SP-SBC [11, 13].

3.7. Effect of Temperature and Adsorption Isotherms. The Cu(II) equilibrium adsorption capacities of SP-SBC (Q_e) at different initial Cu(II) concentrations and temperatures are shown in Figure 10. At the same initial concentration, Q_e increased with increased temperature (15–35°C). This result was due to the increased contact between Cu(II) and SP-SBC at a high temperature. At the same temperature, Q_e increased sharply within the range of low initial Cu(II) concentration (i.e., <200 mg·L^{-1}) ($p < 0.05$) and then gradually reached equilibrium.

To further ascertain the Cu(II)-adsorption behavior of SP-SBC, the experimental data were simulated by the L, F, L-F, and D-R models. Table 4 lists the fitting values of K_L, Q_m, K_f, $1/n$, K_a, n', Q_{mD}, E, and correlation coefficient obtained using the four models. For the L model, K_L can

Table 4: Fitting parameters of four isotherm models.

Temperature	Langmuir			Freundlich		
	K_L ($L \cdot mg^{-1}$)	Q_m ($mg \cdot g^{-1}$)	R^2	K_f ($mg^{(1-n)} \cdot L^n \cdot g^{-1}$)	$1/n$	R^2
15°C	0.17	22.59	0.996	13.63	0.085	0.995
25°C	0.28	26.44	0.994	16.80	0.081	0.996
35°C	0.45	30.52	0.992	19.53	0.080	0.998

Temperature	Langmuir-Freundlich				Dubinin-Radushkevich		
	K_a ($L \cdot mg^{-1}$)	Q_m ($mg \cdot g^{-1}$)	n'	R^2	E ($kJ \cdot mol^{-1}$)	Q_{mD} ($mol \cdot g^{-1}$)	R^2
15°C	0.21	23.22	0.74	0.998	17.51	4.48	0.91
25°C	0.48	31.50	0.33	0.998	21.13	4.89	0.74
35°C	0.52	38.49	0.27	0.999	23.17	5.73	0.91

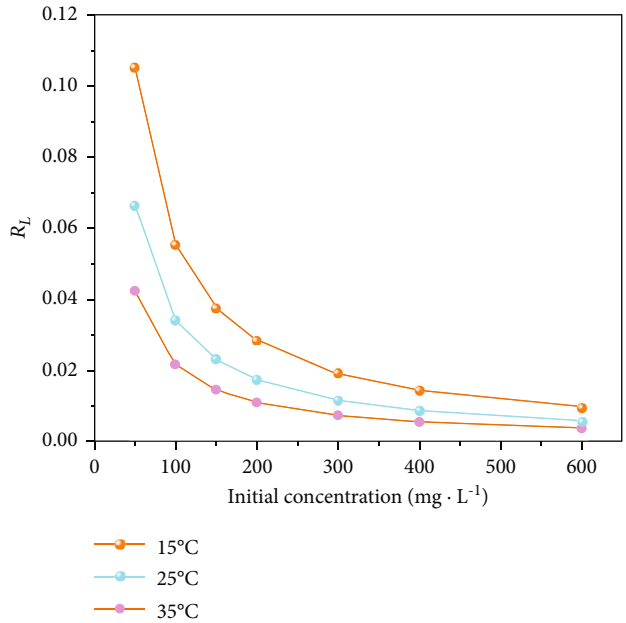

Figure 11: Separation parameters (R_L) for Cu(II) adsorption by SP-SBC at different temperatures and initial Cu(II) concentrations.

be used to calculate the separation parameter (R_L) and reflect the type of isotherm [4, 12], as shown in the following equation.

$$R_L = \frac{1}{1 + C_0 K_L}. \quad (17)$$

Figure 11 shows the R_L values at different temperatures and initial Cu(II) concentrations. The values of R_L were all less than 1, implying that Cu(II) adsorption by SP-SBC was a favorable process [3, 4, 13]. Moreover, with increased the temperature and Cu(II) initial concentration, the R_L value continuously decreased. This result suggested that the Cu(II) adsorption was more favorable at a higher concentration and temperature [80]. For the F model, $1/n$ can reflect the adsorption intensity [56]. If $1/n < 0.5$, the adsorption of the adsorbate is easy, whereas if $1/n > 2$, the adsorption of the adsorbate is difficult [80]. As shown in Table 4, for the different temperatures, the calculated $1/n$ was always less than 0.5, demonstrating that Cu(II) was easily absorbed by SP-SBC. With increased temperature, the value of K_f also increased. A larger value of K_f implies a higher adsorption capacity [79]. Thus, a high temperature was favorable for Cu(II) adsorption; i.e., the Cu(II)-adsorption capacity strengthened with increased the temperature. For the L-F model, the n' values at three temperatures ranged within 0–1, and a higher temperature corresponded with a higher K_a value in this work. The results also demonstrated that Cu(II) adsorption by SP-SBC was a favorable process [81], and the adsorption capability of SP-SBC for Cu(II) was enhanced with increased temperature [82]. For the D-R model, the values of E at all experimental temperatures exceeded 16 $kJ \cdot mol^{-1}$, indicating that Cu(II) adsorption by SP-SBC involved chemical adsorption [83–85].

Figure 10 shows that the experimental data were matched better by the L-F model than the other three models. Furthermore, the L-F model had the highest R^2 among all models (Table 4). Thus, the L-F model was better adapted to fit the isotherms, suggesting that both processes (i.e., the Langmuir and Freundlich processes) were involved in Cu(II) adsorption by SP-SBC. In other words, Cu(II) adsorption was controlled by multiple mechanisms [86], such as ion exchange, precipitation (in Section 3.2) and electrostatic attraction (in Section 3.4). Additionally, the maximum Cu(II)-adsorption capacity of 38.49 $mg \cdot g^{-1}$ was achieved for SP-SBC at 35°C by the L-F model. Table 5 summarizes the Cu(II)-adsorption capacities of different biochars. Compared with these sorbents, SP-SBC had a moderate adsorption capacity. The Cu (II)-adsorption equilibrium time of SP-SBC was also less than those of most adsorbents. Notably, the adsorption capacity of SP-SBC exceeded those of reported commercial activated carbons in Table 5. Overall, SP-SBC is a desirable and effective sorbent for Cu(II) removal from aqueous solutions.

3.8. Fixed-Bed Column Adsorption. Fixed-bed column adsorption can be used to understand the application

Table 5: Cu(II)-adsorption capacities of different biochars.

Biochar	Conditions	Cu(II) maximum adsorption capacity ($mg \cdot g^{-1}$)	References
Corn straw biochar	pH = 5, t = 24 h, T = 22 ∘ C	12.52	[87]
Composted swine manure biochar	pH = 5, t = 24 h, T = 25 ∘ C	21.94	[88]
S. hermaphrodita biochar	pH = 5.5, t = 24 h, T = 22 ∘ C	33.33	[89]
Date seed-derived biochar	pH = 6, t = 24 h, T = 23 ∘ C	26.94	[90]
Miscanthus giganteus biochar	pH = 6, t = 1 h, T = 25 ∘ C	19.72	[91]
Sewage sludge biochar	pH = 5.2, t = 20 h, T = 25 ∘ C	7.32	[36]
Municipal sewage sludge biochar	pH = /, t = 24 h, T = 25 ∘ C	5.34	[37]
Steam-activated giant *Miscanthus* biochar	pH = 6, t = 48 h, T = 20 ∘ C	15.4	[92]
Amino-modified sawdust biochar	pH = 5, t = 200 min, T = 30 ∘ C	17.01	[25]
KOH-activated brewers draft biochar	pH = 5, t = 24 h, T = /	10.30	[93]
$KMnO_4$-modified loofah biochar	pH = 5.5, t = 10 h, T = /	47.64	[71]
Modified date seed biochar with HCl pretreatment	pH = 6, t = 24 h, T = 23 ∘ C	45.12	[24]
NaOH-modified *Opuntia ficus-indica*-activated biochar	pH = 6, t = /, T = 30 ∘ C	49.36	[94]
Commercial activated carbon	pH = 5, t = /, T = 25 ∘ C	19.21	[95]
Commercial activated carbon	pH = 4, t = 4 h, T = 25 ∘ C	6.9	[96]
Commercial activated carbon	pH = 6.5, t = 1 h, T = 22 ∘ C	13.7	[97]
SP-SBC	pH = 5, t = 12 h, T = 35 ∘ C	38.49	This study

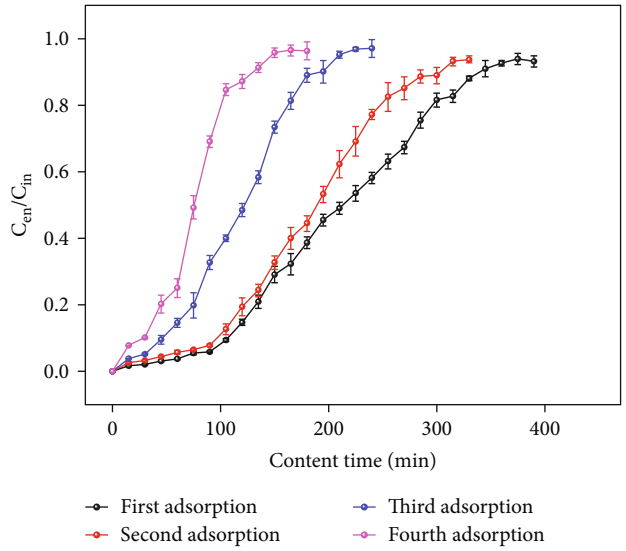

Figure 12: Breakthrough curves of four adsorption–desorption cycles in the fixed-bed column experiment.

potential of SP-SBC and offer support for the large-scale treatment of real copper-containing wastewater by SP-SBC [98]. Figure 12 and Table 6 show the breakthrough curves and the corresponding calculated parameters of four adsorption–desorption cycles in the fixed-bed column experiment, respectively. The values of q_{ec}, M', and V_{eff} in the first cycle were 8.528 $mg \cdot g^{-1}$, 153.5 mg, and 5175 mL, respectively, indicating that SP-SBC can be used for fixed-bed column

Table 6: Adsorption parameters acquired by fixed-bed column adsorption in four adsorption–desorption cycles.

Cycle	t_b* (min)	t_e (min)	V_{eff} (mL)	M (mg)	M' (mg)	q_{ec} ($mg \cdot g^{-1}$)
1	110	345	5175	258.75	153.5	8.528
2	95	310	4650	232.50	133.71	7.428
3	50	195	2925	146.25	82.49	4.583
4	30	125	1875	93.75	50.29	2.794

*t_b is the breakthrough time (min), which is the corresponding time when $C_t/C_0 = 0.1$.

adsorption. With the number of cycles increasing, the slope of the breakout curve increased gradually, indicating that the breakthrough ($C_t/C_0 = 0.1$) and saturation ($C_t/C_0 = 0.9$) points came earlier, and the values of M, M', V_{eff}, and q_{ec} decreased. These changes may be due to the inactivation of adsorption sites on the surface of SP-SBC during the adsorption–desorption cycles. After four adsorption–desorption cycles, q_{ec} was still 2.794 $mg \cdot g^{-1}$, indicating that SP-SBC can be reused at least four times. Considering the large sewage sludge production in China ($>3 \times 10^7$ *tons per year*), the relatively simple preparation procedures, and the desired adsorption performance in the fixed-bed column adsorption, SP-SBC has a good application potential to treat copper-containing wastewater. Nevertheless, to effectively guide the practical application of SP-SBC, the following works need to be carried out: (i) optimization of adsorption-operating parameters to determine the optimum adsorption

conditions; (ii) evaluation of the desorption effect of various desorbents, such as H_2SO_4, HNO_3, and EDTA, to select the effective desorbents; and (iii) design of feasible preparation procedures of SP-SBC from the perspective of industrial production to provide technical guidance for the market promotion of SP-SBC.

4. Conclusions

$Na_4P_2O_7$-modified biochar (SP-SBC) was successfully prepared by a simple one-pot method. Compared with SBC, the Cu(II)-adsorption capacity of SP-SBC improved 4.55 times. The Cu(II)-adsorption process of SP-SBC can be better described by the pseudo-second-order and Langmuir-Freundlich models. Cu(II) adsorption by SP-SBC involved ion exchange, electrostatic attraction, and precipitation. For Cu(II) adsorption, SP-SBC gained the maximum adsorption capacity of 38.49 $mg \cdot g^{-1}$ at 35°C, which was higher than those of some reported commercial activated carbons. The fixed-bed column experiment indicated that SP-SBC can be used at least four times and had a good application potential for the treatment of copper-containing wastewater. Overall, SP-SBC can serve as an alternative sorbent to effectively remove Cu(II) from aqueous solutions. For the practical application of SP-SBC, the optimization of adsorption-operation parameters, evaluation of the desorption effect of various desorbents, and design of a feasible industrial-production scheme are required.

Data Availability

All data generated or analyzed during this study are included in this published article.

Conflicts of Interest

The authors have no competing interests to declare that are relevant to the content of this article.

Authors' Contributions

Liangqian Fan, Xianda Wang, and Jiaxin Miao contributed equally to this work and should be considered as co-first authors.

Acknowledgments

This work was financially supported by the Scientific Research Innovation Team Project of Sichuan Provincial Department of Education (No. 16TD0006).

References

[1] R. R. Karri, G. Ravindran, and M. H. Dehghani, "Wastewater–sources, toxicity, and their consequences to human health," in *Soft computing techniques in solid waste and wastewater management*, pp. 3–33, Elsevier, 2021.

[2] M. H. Dehghani, G. A. Omrani, and R. R. Karri, "Solid waste–sources, toxicity, and their consequences to human health," in *Soft computing techniques in solid waste and wastewater management*, pp. 205–213, Elsevier, 2021.

[3] K. L. Bhowmik, A. Debnath, R. K. Nath, and B. Saha, "Synthesis of $MnFe_2O_4$ and Mn_3O_4 magnetic nano-composites with enhanced properties for adsorption of Cr(VI): artificial neural network modeling," *Water Science and Technology*, vol. 76, no. 12, pp. 3368–3378, 2017.

[4] A. Debnath, A. Bera, K. K. Chattopadhyay, and B. Saha, "Facile additive-free synthesis of hematite nanoparticles for enhanced adsorption of hexavalent chromium from aqueous media: kinetic, isotherm, and thermodynamic study," *Inorganic and Nano-Metal Chemistry*, vol. 47, no. 12, pp. 1605–1613, 2017.

[5] Y. Yan, X. Liang, J. Ma, and J. Shen, "Rapid removal of copper from wastewater by Fe-based amorphous alloy," *Intermetallics*, vol. 124, article 106849, 2020.

[6] Q. Wang, L. Li, L. Kong et al., "Compressible amino-modified carboxymethyl chitosan aerogel for efficient Cu(II) adsorption from wastewater," *Separation and Purification Technology*, vol. 293, article 121146, 2022.

[7] H. Zhang, J. Chen, S. Ni, C. Bie, H. Zhi, and X. Sun, "A clean process for selective recovery of copper from industrial wastewater by extraction-precipitation with p-tert-octyl phenoxy acetic acid," *Journal of Environmental Management*, vol. 304, article 114164, 2022.

[8] Y. Li, B. Pan, H. Miao, H. Xu, X. Liu, and G. Shi, "Single and binary dye adsorption of methylene blue and methyl orange in alcohol aqueous solution via rice husk based activated carbon: kinetics and equilibrium studies," *Chemical Research in Chinese Universities*, vol. 36, no. 6, pp. 1272–1278, 2020.

[9] M. Feng, S. Yu, P. Wu, Z. Wang, S. Liu, and J. Fu, "Rapid, high-efficient and selective removal of cationic dyes from wastewater using hollow polydopamine microcapsules: isotherm, kinetics, thermodynamics and mechanism," *Applied Surface Science*, vol. 542, article 148633, 2021.

[10] W. Tala and S. Chantara, "Use of spent coffee ground biochar as ambient PAHs sorbent and novel extraction method for GC-MS analysis," *Environmental Science and Pollution Research*, vol. 26, no. 13, pp. 13025–13040, 2019.

[11] L. P. Lingamdinne, R. R. Karri, M. R. Khan, Y. Chang, and J. R. Koduru, "Evaluation of surface phenomena of magnetic biomass for dye removal via surface modeling," *Journal of Environmental Chemical Engineering*, vol. 105953, no. 5, article 105953, 2021.

[12] B. Saha, A. Debnath, and B. Saha, "Fabrication of PANI@Fe–Mn–Zr hybrid material and assessments in sono-assisted adsorption of methyl red dye: uptake performance and response surface optimization," *Journal of the Indian Chemical Society*, vol. 99, no. 9, article 100635, 2022.

[13] P. Das and A. Debnath, "Fabrication of $MgFe_2O_4$/polyaniline nanocomposite for amputation of methyl red dye from water: isotherm modeling, kinetic and cost analysis," *Journal of Dispersion Science and Technology*, vol. 43, pp. 1–12, 2022.

[14] B. Saha, A. Debnath, and B. Saha, "Evaluation of Fe–Mn–Zr trimetal oxide/polyaniline nanocomposite as potential adsorbent for abatement of toxic dye from aqueous solution," in *Polymer Technology in dye-Containing Wastewater*, pp. 15–37, Springer Nature Singapore, Singapore, 2022.

[15] L. P. Lingamdinne, J. Choi, G. K. R. Angaru et al., "Magnetic-watermelon rinds biochar for uranium-contaminated water treatment using an electromagnetic semi-batch column with removal mechanistic investigations," *Chemosphere*, vol. 286, article 131776, Part 2, 2022.

[16] M. N. Hairuddin, N. M. Mubarak, M. Khalid, E. C. Abdullah, R. Walvekar, and R. R. Karri, "Magnetic palm kernel biochar potential route for phenol removal from wastewater," *Environmental Science and Pollution Research*, vol. 26, no. 34, pp. 35183–35197, 2019.

[17] Z. Meng, T. Xu, S. Huang, H. Ge, W. Mu, and Z. Lin, "Effects of competitive adsorption with Ni(II) and Cu(II) on the adsorption of Cd(II) by modified biochar co-aged with acidic soil," *Chemosphere*, vol. 293, article 133621, 2022.

[18] X. Wang, X. Li, G. Liu et al., "Mixed heavy metal removal from wastewater by using discarded mushroom-stick biochar: adsorption properties and mechanisms," *Environmental Science: Processes & Impacts*, vol. 21, no. 3, pp. 584–592, 2019.

[19] T. Chi, J. Zuo, and F. Liu, "Performance and mechanism for cadmium and lead adsorption from water and soil by corn straw biochar," *Frontiers of Environmental Science & Engineering*, vol. 11, no. 2, p. 15, 2017.

[20] Z. Mahdi, Q. J. Yu, and A. El Hanandeh, "Competitive adsorption of heavy metal ions (Pb^{2+}, Cu^{2+}, and Ni^{2+}) onto date seed biochar: batch and fixed bed experiments," *Separation Science and Technology*, vol. 54, no. 6, pp. 888–901, 2019.

[21] Z. Zhou, Z. Xu, Q. Feng et al., "Effect of pyrolysis condition on the adsorption mechanism of lead, cadmium and copper on tobacco stem biochar," *Journal of Cleaner Production*, vol. 187, pp. 996–1005, 2018.

[22] F. Wu, L. Chen, P. Hu, Y. Wang, J. Deng, and B. Mi, "Industrial alkali lignin-derived biochar as highly efficient and low-cost adsorption material for Pb(II) from aquatic environment," *Bioresource Technology*, vol. 322, article 124539, 2021.

[23] R. Katiyar, A. K. Patel, T. Nguyen, R. R. Singhania, C. Chen, and C. Dong, "Adsorption of copper (II) in aqueous solution using biochars derived from *Ascophyllum nodosum* seaweed," *Bioresource Technology*, vol. 328, article 124829, 2021.

[24] Z. Mahdi, A. E. Hanandeh, and Q. J. Yu, "Preparation, characterization and application of surface modified biochar from date seed for improved lead, copper, and nickel removal from aqueous solutions," *Journal of Environmental Chemical Engineering*, vol. 7, no. 5, article 103379, 2019.

[25] G. Yang and H. Jiang, "Amino modification of biochar for enhanced adsorption of copper ions from synthetic wastewater," *Water Research*, vol. 48, pp. 396–405, 2014.

[26] H. Wang, B. Gao, S. Wang, J. Fang, Y. Xue, and K. Yang, "Removal of Pb(II), Cu(II), and Cd(II) from aqueous solutions by biochar derived from $KMnO_4$ treated hickory wood," *Bioresource Technology*, vol. 197, pp. 356–362, 2015.

[27] F. Wang, L. Jin, C. Guo et al., "Enhanced heavy metals sorption by modified biochars derived from pig manure," *Science of the Total Environment*, vol. 786, article 147595, 2021.

[28] S. Bashir, J. Zhu, Q. Fu, and H. Hu, "Comparing the adsorption mechanism of Cd by rice straw pristine and KOH-modified biochar," *Environmental Science and Pollution Research*, vol. 25, no. 12, pp. 11875–11883, 2018.

[29] J. Xiong, M. Zhou, C. Qu et al., "Quantitative analysis of Pb adsorption on sulfhydryl-modified biochar," *Biochar*, vol. 3, no. 1, pp. 37–49, 2021.

[30] Y. Wang and R. Liu, "H_2O_2 treatment enhanced the heavy metals removal by manure biochar in aqueous solutions," *Science of the Total Environment*, vol. 628-629, pp. 1139–1148, 2018.

[31] J. Song, S. Zhang, G. Li, Q. Du, and F. Yang, "Preparation of montmorillonite modified biochar with various temperatures and their mechanism for Zn ion removal," *Journal of Hazardous Materials*, vol. 391, article 121692, 2020.

[32] G. Zhou, Y. Gu, H. Yuan, Y. Gong, and Y. Wu, "Selecting sustainable technologies for disposal of municipal sewage sludge using a multi-criterion decision-making method: a case study from China," *Resources Conservation and Recycling*, vol. 161, article 104881, 2020.

[33] S. Zhang, F. Wang, Z. Mei, L. Lv, and Y. Chi, "Status and development of sludge incineration in China," *Waste and Biomass Valorization*, vol. 12, no. 7, pp. 3541–3574, 2021.

[34] K. Bondarczuk, A. Markowicz, and Z. Piotrowska-Seget, "The urgent need for risk assessment on the antibiotic resistance spread via sewage sludge land application," *Environment International*, vol. 87, pp. 49–55, 2016.

[35] T. Chen, Y. Zhang, H. Wang et al., "Influence of pyrolysis temperature on characteristics and heavy metal adsorptive performance of biochar derived from municipal sewage sludge," *Bioresource Technology*, vol. 164, pp. 47–54, 2014.

[36] T. Shen, Y. Tang, X. Lu, and Z. Meng, "Mechanisms of copper stabilization by mineral constituents in sewage sludge biochar," *Journal of Cleaner Production*, vol. 193, pp. 185–193, 2018.

[37] Z. Dan, L. Dan, G. Fengxiang, L. Mengke, and L. Xianping, "Effects of biochar-derived sewage sludge on heavy metal adsorption and immobilization in soils," *International Journal of Environmental Research and Public Health*, vol. 14, no. 7, p. 681, 2017.

[38] L. Gao, J. Deng, G. Huang et al., "Relative distribution of Cd^{2+} adsorption mechanisms on biochars derived from rice straw and sewage sludge," *Bioresource Technology*, vol. 272, pp. 114–122, 2019.

[39] T. Chen, Z. Zhou, S. Xu, H. Wang, and W. Lu, "Adsorption behavior comparison of trivalent and hexavalent chromium on biochar derived from municipal sludge," *Bioresource Technology*, vol. 190, pp. 388–394, 2015.

[40] M. Wu, B. Liu, J. Li, X. Su, W. Liu, and X. Li, "Influence of pyrolysis temperature on sludge biochar: the ecological risk assessment of heavy metals and the adsorption of Cd(II)," *Environmental Science and Pollution Research*, 2022.

[41] M. Zhao, Y. Dai, M. Zhang et al., "Mechanisms of Pb and/or Zn adsorption by different biochars: biochar characteristics, stability, and binding energies," *Science of the Total Environment*, vol. 717, article 136894, 2020.

[42] Y. Chen, M. Li, Y. Li et al., "Hydroxyapatite modified sludge-based biochar for the adsorption of Cu^{2+} and Cd^{2+}: adsorption behavior and mechanisms," *Bioresource Technology*, vol. 321, article 124413, 2021.

[43] K. M. Smith, G. D. Fowler, S. Pullket, and N. J. D. Graham, "Sewage sludge-based adsorbents: a review of their production, properties and use in water treatment applications," *Water Research*, vol. 43, no. 10, pp. 2569–2594, 2009.

[44] C. Santhosh, E. Daneshvar, K. M. Tripathi et al., "Synthesis and characterization of magnetic biochar adsorbents for the removal of Cr(VI) and acid orange 7 dye from aqueous solution," *Environmental Science and Pollution Research*, vol. 27, no. 26, pp. 32874–32887, 2020.

[45] W. Zuo, C. Chen, H. Cui, and M. Fu, "Enhanced removal of Cd(II) from aqueous solution using $CaCO_3$ nanoparticle modified sewage sludge biochar," *RSC Advances*, vol. 7, no. 26, pp. 16238–16243, 2017.

[46] N. Zhao, B. Li, H. Huang, X. Lv, M. Zhang, and L. Cao, "Modification of kelp and sludge biochar by TMT-102 and NaOH

for cadmium adsorption," *Journal of the Taiwan Institute of Chemical Engineers*, vol. 116, pp. 101–111, 2020.

[47] L. Yang, L. He, J. Xue et al., "Highly efficient nickel (II) removal by sewage sludge biochar supported α-Fe_2O_3 and α-FeOOH: sorption characteristics and mechanisms," *PLoS One*, vol. 14, no. 6, article e218114, 2019.

[48] J. Wang, T. Wang, Q. Zhu et al., "Preparation of a novel sludge-derived biochar by K_2FeO_4 conditioning to enhance the removal of Pb^{2+}," *Colloid and Interface Science Communications*, vol. 42, article 100417, 2021.

[49] I. I. Shahib, J. Ifthikar, D. T. Oyekunle et al., "Influences of chemical treatment on sludge derived biochar; physicochemical properties and potential sorption mechanisms of lead (II) and methylene blue," *Journal of Environmental Chemical Engineering*, vol. 10, no. 3, article 107725, 2022.

[50] K. Phoungthong and T. Suwunwong, "Magnetic biochar derived from sewage sludge of concentrated natural rubber latex (CNRL) for the removal of Al^{3+} and Cu^{2+} ions from wastewater," *Research on Chemical Intermediates*, vol. 46, no. 1, pp. 385–407, 2020.

[51] S. Tang, N. Shao, C. Zheng, F. Yan, and Z. Zhang, "Amino-functionalized sewage sludge-derived biochar as sustainable efficient adsorbent for Cu(II) removal," *Waste Management*, vol. 90, pp. 17–28, 2019.

[52] L. Fan, J. Miao, J. Yang et al., "Invasive plant-crofton weed as adsorbent for effective removal of copper from aqueous solution," *Environmental Technology & Innovation*, vol. 26, article 102280, 2022.

[53] N. Delgado, A. Capparelli, A. Navarro, and D. Marino, "Pharmaceutical emerging pollutants removal from water using powdered activated carbon: study of kinetics and adsorption equilibrium," *Journal of Environmental Management*, vol. 236, pp. 301–308, 2019.

[54] N. Slyusarenko, M. Gerasimova, M. Atamanova, A. Plotnikov, and E. Slyusareva, "Adsorption of eosin Y on polyelectrolyte complexes based on chitosan and arabinogalactan sulfate," *Colloids and Surfaces A: Physicochemical and Engineering Aspects*, vol. 610, article 125731, 2021.

[55] R. R. Karri, J. N. Sahu, and B. C. Meikap, "Improving efficacy of Cr (VI) adsorption process on sustainable adsorbent derived from waste biomass (sugarcane bagasse) with help of ant colony optimization," *Industrial Crops and Products*, vol. 143, article 111927, 2020.

[56] R. R. Karri, J. N. Sahu, and N. S. Jayakumar, "Optimal isotherm parameters for phenol adsorption from aqueous solutions onto coconut shell based activated carbon: error analysis of linear and non-linear methods," *Journal of the Taiwan Institute of Chemical Engineers*, vol. 80, pp. 472–487, 2017.

[57] F. Wang, J. Yu, Z. Zhang, Y. Xu, and R. Chi, "An amino-functionalized ramie stalk-based adsorbent for highly effective Cu^{2+} removal from water: adsorption performance and mechanism," *Process Safety and Environmental Protection*, vol. 117, pp. 511–522, 2018.

[58] A. Abdolali, H. H. Ngo, W. Guo et al., "Application of a breakthrough biosorbent for removing heavy metals from synthetic and real wastewaters in a lab-scale continuous fixed-bed column," *Bioresource Technology*, vol. 229, pp. 78–87, 2017.

[59] J. Jin, Y. Li, J. Zhang et al., "Influence of pyrolysis temperature on properties and environmental safety of heavy metals in biochars derived from municipal sewage sludge," *Journal of Hazardous Materials*, vol. 320, pp. 417–426, 2016.

[60] S. Ho, Y. Chen, Z. Yang, D. Nagarajan, J. Chang, and N. Ren, "High-efficiency removal of lead from wastewater by biochar derived from anaerobic digestion sludge," *Bioresource Technology*, vol. 246, pp. 142–149, 2017.

[61] F. Ma, J. Dai, Z. Fu et al., "Biochar for asphalt modification: a case of high-temperature properties improvement," *Science of the Total Environment*, vol. 804, article 150194, 2022.

[62] W. Wu, M. Yang, Q. Feng et al., "Chemical characterization of rice straw-derived biochar for soil amendment," *Biomass and Bioenergy*, vol. 47, pp. 268–276, 2012.

[63] N. Hagemann, E. Subdiaga, S. Orsetti et al., "Effect of biochar amendment on compost organic matter composition following aerobic composting of manure," *Science of the Total Environment*, vol. 613-614, pp. 20–29, 2018.

[64] C. He, X. He, J. Li et al., "The spectral characteristics of biochar-derived dissolved organic matter at different pyrolysis temperatures," *Journal of Environmental Chemical Engineering*, vol. 9, no. 5, article 106075, 2021.

[65] S. Chellappan, V. Nair, V. Sajith, and K. Aparna, "Synthesis, optimization and characterization of biochar based catalyst from sawdust for simultaneous esterification and transesterification," *Chinese Journal of Chemical Engineering*, vol. 26, no. 12, pp. 2654–2663, 2018.

[66] F. V. Hackbarth, F. Girardi, S. M. A. G. de Souza, A. D. Souza, R. Boaventura, and V. Vilar, "Marine macroalgae *Pelvetia canaliculata* (*Phaeophyceae*) as a natural cation exchanger for cadmium and lead ions separation in aqueous solutions," *Chemical Engineering Journal*, vol. 242, pp. 294–305, 2014.

[67] L. Zhao, X. Cao, O. Masek, and A. Zimmerman, "Heterogeneity of biochar properties as a function of feedstock sources and production temperatures," *Journal of Hazardous Materials*, vol. 256-257, pp. 1–9, 2013.

[68] Y. Chen, Y. Liu, Y. Li et al., "Novel magnetic pomelo peel biochar for enhancing Pb(II) and Cu(II) adsorption: performance and mechanism," *Water, Air, & Soil Pollution*, vol. 231, no. 8, p. 404, 2020.

[69] S. Zhao, N. Ta, and X. Wang, "Absorption of Cu(II) and Zn(II) from aqueous solutions onto biochars derived from apple tree branches," *Energies*, vol. 13, no. 13, p. 3498, 2020.

[70] H. H. Han, A. Kim, T. Kim, and Y. Bae, "Facile Cu(I) loading for adsorptive C_3H_6/C_3H_8 separation through double Cu(II) salts incorporation within pores with unsaturated Fe(II) sites," *Bulletin of the Korean Chemical Society*, vol. 42, no. 3, pp. 471–476, 2021.

[71] F. Zhao, R. Shan, J. Gu, Y. Zhang, H. Yuan, and Y. Chen, "Magnetically recyclable loofah biochar by $KMnO_4$ modification for adsorption of Cu(II) from aqueous solutions," *ACS Omega*, vol. 7, no. 10, pp. 8844–8853, 2022.

[72] K. Jung, S. Y. Lee, and Y. J. Lee, "Hydrothermal synthesis of hierarchically structured birnessite-type MnO_2/biochar composites for the adsorptive removal of Cu(II) from aqueous media," *Bioresource Technology*, vol. 260, pp. 204–212, 2018.

[73] Z. Lu, H. Zhang, A. Shahab et al., "Comparative study on characterization and adsorption properties of phosphoric acid activated biochar and nitrogen-containing modified biochar employing eucalyptus as a precursor," *Journal of Cleaner Production*, vol. 303, article 127046, 2021.

[74] J. Deng, Y. Liu, S. Liu et al., "Competitive adsorption of Pb(II), Cd(II) and Cu(II) onto chitosan-pyromellitic dianhydride modified biochar," *Journal of Colloid and Interface Science*, vol. 506, pp. 355–364, 2017.

[75] V. Bernal, L. Giraldo, and J. C. Moreno-Piraján, "Thermodynamic analysis of acetaminophen and salicylic acid adsorption onto granular activated carbon: importance of chemical surface and effect of ionic strength," *Thermochimica Acta*, vol. 683, article 178467, 2020.

[76] Y. Xiao, Y. Xue, F. Gao, and A. Mosa, "Sorption of heavy metal ions onto crayfish shell biochar: effect of pyrolysis temperature, pH and ionic strength," *Journal of the Taiwan Institute of Chemical Engineers*, vol. 80, pp. 114–121, 2017.

[77] Y. Chen, B. Wang, J. Xin, P. Sun, and D. Wu, "Adsorption behavior and mechanism of Cr(VI) by modified biochar derived from *Enteromorpha prolifera*," *Ecotoxicology and Environmental Safety*, vol. 164, pp. 440–447, 2018.

[78] G. Tan, W. Sun, Y. Xu, H. Wang, and N. Xu, "Sorption of mercury (II) and atrazine by biochar, modified biochars and biochar based activated carbon in aqueous solution," *Bioresource Technology*, vol. 211, pp. 727–735, 2016.

[79] Z. Chen, T. Liu, J. Tang et al., "Characteristics and mechanisms of cadmium adsorption from aqueous solution using lotus seedpod-derived biochar at two pyrolytic temperatures," *Environmental Science and Pollution Research*, vol. 25, no. 12, pp. 11854–11866, 2018.

[80] S. Fan, Y. Wang, Z. Wang, J. Tang, J. Tang, and X. Li, "Removal of methylene blue from aqueous solution by sewage sludge-derived biochar: adsorption kinetics, equilibrium, thermodynamics and mechanism," *Journal of Environmental Chemical Engineering*, vol. 5, no. 1, pp. 601–611, 2017.

[81] R. Marouf, N. Khelifa, K. Marouf-Khelifa, J. Schott, and A. Khelifa, "Removal of pentachlorophenol from aqueous solutions by dolomitic sorbents," *Journal of Colloid and Interface Science*, vol. 297, no. 1, pp. 45–53, 2006.

[82] Z. Zhao, S. Wang, Y. Yang, X. Li, J. Li, and Z. Li, "Competitive adsorption and selectivity of benzene and water vapor on the microporous metal organic frameworks (HKUST-1)," *Chemical Engineering Journal*, vol. 259, pp. 79–89, 2015.

[83] J. Li, G. Yu, L. Pan et al., "Study of ciprofloxacin removal by biochar obtained from used tea leaves," *Journal of Environmental Sciences*, vol. 73, pp. 20–30, 2018.

[84] H. Yan, W. Zhang, X. Kan et al., "Sorption of methylene blue by carboxymethyl cellulose and reuse process in a secondary sorption," *Colloids and Surfaces A: Physicochemical and Engineering Aspects*, vol. 380, no. 1-3, pp. 143–151, 2011.

[85] Ş. S. Bayazit, E. Kurtulbaş, M. Bilgin, and S. Şahin, "Decontamination of endocrine disruptors from water by graphene nanoplatelet/UiO-66 nanocomposites," *Environmental Nanotechnology, Monitoring & Management*, vol. 18, article 100733, 2022.

[86] M. Zhang, J. Yang, H. Wang, Q. Lv, and J. Xue, "Enhanced removal of phosphate from aqueous solution using Mg/Fe modified biochar derived from excess activated sludge: removal mechanism and environmental risk," *Environmental Science and Pollution Research*, vol. 28, no. 13, pp. 16282–16297, 2021.

[87] X. Chen, G. Chen, L. Chen et al., "Adsorption of copper and zinc by biochars produced from pyrolysis of hardwood and corn straw in aqueous solution," *Bioresource Technology*, vol. 102, no. 19, pp. 8877–8884, 2011.

[88] J. Meng, X. Feng, Z. Dai, X. Liu, J. Wu, and J. Xu, "Adsorption characteristics of Cu(II) from aqueous solution onto biochar derived from swine manure," *Environmental Science and Pollution Research*, vol. 21, no. 11, pp. 7035–7046, 2014.

[89] A. Bogusz, P. Oleszczuk, and R. Dobrowolski, "Application of laboratory prepared and commercially available biochars to adsorption of cadmium, copper and zinc ions from water," *Bioresource Technology*, vol. 196, pp. 540–549, 2015.

[90] Z. Mahdi, Q. J. Yu, and A. E. Hanandeh, "Investigation of the kinetics and mechanisms of nickel and copper ions adsorption from aqueous solutions by date seed derived biochar," *Journal of Environmental Chemical Engineering*, vol. 6, no. 1, pp. 1171–1181, 2018.

[91] A. Cibati, B. Foereid, A. Bissessur, and S. Hapca, "Assessment of *Miscanthus* × *giganteus* derived biochar as copper and zinc adsorbent: study of the effect of pyrolysis temperature, pH and hydrogen peroxide modification," *Journal of Cleaner Production*, vol. 162, pp. 1285–1296, 2017.

[92] T. Shim, J. Yoo, C. Ryu, Y. Park, and J. Jung, "Effect of steam activation of biochar produced from a giant Miscanthus on copper sorption and toxicity," *Bioresource Technology*, vol. 197, pp. 85–90, 2015.

[93] L. Trakal, R. Šigut, H. Šillerová, D. Faturíková, and M. Komárek, "Copper removal from aqueous solution using biochar: effect of chemical activation," *Arabian Journal of Chemistry*, vol. 7, no. 1, pp. 43–52, 2014.

[94] M. Choudhary, R. Kumar, and S. Neogi, "Activated biochar derived from *Opuntia ficus-indica* for the efficient adsorption of malachite green dye, Cu^{+2} and Ni^{+2} from water," *Journal of Hazardous Materials*, vol. 392, article 122441, 2020.

[95] M. L. Huang, C. Wang, and S. Q. Liu, "Adsorption of Cu and Ni ions from aqueous solutions by commercial activated carbon and the reutilization in glass coloration," *Journal of Wuhan University of Technology-Materials Science*, vol. 34, no. 1, pp. 41–46, 2019.

[96] E. Pehlivan and S. Cetin, "Application of fly ash and activated carbon in the removal of Cu^{2+} and Ni^{2+} ions from aqueous solutions," *Energy Sources Part A-Recovery Utilization and Environmental Effects*, vol. 30, no. 13, pp. 1153–1165, 2008.

[97] E. Safaei, N. S. Langeroodi, and E. Baher, "Investigation of removal of Cu(II) ions by commercial activated carbon: equilibrium and thermodynamic studies," *Protection of Metals and Physical Chemistry of Surfaces*, vol. 55, no. 1, pp. 28–33, 2019.

[98] M. Zhang, M. Ahmad, M. I. Al-Wabel et al., "Adsorptive removal of trichloroethylene in water by crop residue biochars pyrolyzed at contrasting temperatures: continuous fixed-bed experiments," *Journal of Chemistry*, vol. 2015, Article ID 647072, 6 pages, 2015.